

Spectroscopic studies of Yb³⁺-doped rare earth orthosilicate crystals

This article has been downloaded from IOPscience. Please scroll down to see the full text article.

2004 J. Phys.: Condens. Matter 16 4579

(<http://iopscience.iop.org/0953-8984/16/25/015>)

View [the table of contents for this issue](#), or go to the [journal homepage](#) for more

Download details:

IP Address: 129.252.86.83

The article was downloaded on 27/05/2010 at 15:38

Please note that [terms and conditions apply](#).

Spectroscopic studies of Yb³⁺-doped rare earth orthosilicate crystals

S Campos¹, A Denoyer¹, S Jandl¹, B Viana², D Vivien², P Loiseau²
and B Ferrand³

¹ Département de Physique, Université de Sherbrooke, Sherbrooke, QC, J1K 2R1, Canada

² Laboratoire de Chimie Appliquée de l'état Solide, ENSCP, 11 rue Pierre et Marie Curie, 75231 Paris cedex 05, France

³ LETI/DOPT/STCO/Laboratoire Cristallogénèse Appliquée, CEA-Grenoble, 17 rue des Martyrs, 38054 Grenoble cedex 9, France

Received 17 February 2004

Published 11 June 2004

Online at stacks.iop.org/JPhysCM/16/4579

doi:10.1088/0953-8984/16/25/015

Abstract

Infrared transmission and Raman scattering have been used to study Raman active phonons and crystal-field excitations in Yb³⁺-doped yttrium, lutetium and scandium orthosilicate crystals (Y₂SiO₅ (YSO), Lu₂SiO₅ (LSO) and Sc₂SiO₅ (SSO)), which belong to the same C_{2h}⁶ crystallographic space group. Energy levels of the Yb³⁺ ion ²F_{5/2} manifold are presented. In the three hosts, Yb³⁺ ions experience high crystal field strength, particularly in Yb:SSO. Satellites in the infrared transmission spectra have been detected for the first time in the Yb³⁺-doped rare earth orthosilicates. They could be attributed to perturbed Yb³⁺ sites of the lattices or to magnetically coupled Yb³⁺ pairs.

1. Introduction

In recent years, Yb³⁺-based laser materials emitting around 1 μm are becoming of great importance as possible substitutes to the Nd³⁺ based solid lasers [1–3]. They actually present several advantages such as a smaller quantum defect, resulting in lower thermal loading of the laser rod, and a simpler electronic structure with just two manifold levels (²F_{7/2} and ²F_{5/2}) preventing self-quenching by cross relaxation and up-conversion parasitic effects. In addition, the Yb³⁺ concentration can be made very high (tens of %), and for this ion the radiative lifetime is longer as compared to Nd³⁺ activated solids, leading to possible device miniaturization which can be pumped using 900–980 nm InGaAs laser diodes. There are however some drawbacks, among which is the quasi-three-level type laser operation, since the ground state manifold is also the laser terminal level. It follows that the crystal field splitting of the ²F_{7/2} ground state is needed to be large.

Laser action in Yb:Y₂SiO₅ (Yb:YSO) was first reported in 2000, using a titanium sapphire laser as pump source [4], with a slope efficiency of ~50% [5]. Later on, output power

reaching 2.1 W (CW) was obtained under diode pumping with an optical to optical efficiency of $\sim 30\%$ [6]. The Yb:YSO crystal has several advantages over other Yb-based lasers. The splitting of the $\text{Yb}^{3+} {}^2\text{F}_{7/2}$ ground state (715 and 964 cm^{-1} [7] for the two Y^{3+} sites that can be substituted by Yb^{3+}) is rather large and the thermal conductivity ($\sim 4.4 \text{ W m}^{-1} \text{ K}^{-1}$) is one of the highest among Yb^{3+} -doped hosts [8]. This value can be compared to $6 \text{ W m}^{-1} \text{ K}^{-1}$ in the 15% Yb:YAG laser material [9].

In Yb:YSO free running laser emission occurs at 1042, 1059 or 1082 nm [5], depending on the output mirror transmission, and the laser can be forced to oscillate at 1003.4 nm (with a tunability range extending from 1001.3 to 1044 nm) [10]. Emission at 1003.4 nm is interesting because it can be frequency doubled to 501.7 nm, a wavelength which corresponds to the narrowest iodine absorption line, thus allowing us to build an ultra-stable laser source.

In order to account for these laser properties, it is necessary to determine the Yb^{3+} energy level diagram in the YSO host. Previous investigations of Yb^{3+} :YSO [5, 7] and its parent compound Yb^{3+} : Sc_2SiO_5 (Yb:SSO) [8] have been published recently. However, the line assignments are not trivial since the Yb^{3+} ions give rise to strong electron–phonon coupling [1, 2, 11] which generates a large number of phonon replicas in the absorption spectrum. In this paper, we report high-resolution infrared and Raman spectroscopy measurements as a function of temperature in Yb:YSO, Yb: Lu_2SiO_5 (Yb:LSO) and Yb:SSO single crystals. The objectives of our study are (i) to determine the Raman active phonons of the host materials, (ii) to identify the Yb^{3+} ion crystal field (CF) levels and their vibronic sidebands in various host materials and (iii) to highlight the occurrence of several satellites associated with the main absorption lines which may be assigned to perturbed Yb^{3+} centres or to Yb^{3+} – Yb^{3+} pair interactions as already reported in Nd^{3+} : YVO_4 and Nd^{3+} : YLiF_4 for the Nd^{3+} – Nd^{3+} pair exchange interactions [6–8].

2. Crystal structure and experimental settings

YSO, LSO and SSO crystallize in the $C2/c$ (C_{2h}^6) monoclinic space group, the Y (Lu, Sc) dielectric axis being along the b axis unit cell direction. Several crystal structures, differing slightly in the atomic positions, can be found in the literature for these rare earth orthosilicates. In the following, structure descriptions of [12] and [13] are used for YSO and LSO respectively. The detailed structure of SSO is unknown, although the unit cell parameters have been reported [14]. Ytterbium ions enter the two non-equivalent and equally populated distorted rare earth (RE) sites of these host lattices, with coordination number $(6 + 1)$ and 6 for RE(I) and RE(II) respectively and C_1 symmetry in both cases. The rare earth ions are arranged in compact chains running along the c axis while the RE coordination polyhedra share edges in the chains that are linked together by SiO_4 tetrahedra.

The studied single crystals, YSO, 5% and 15% Yb:YSO, 6% Yb:LSO and 1% Yb:SSO, were grown either from the melt using the Czochralski technique (YSO, 5% and 15% Yb:YSO and 6% Yb:LSO) or the zone melting method (1% Yb:SSO). The samples were subsequently cut and polished to provide homogeneous surfaces.

Low temperature micro-Raman backscattering spectra were recorded using a Labram 800 spectrometer equipped with a charge-coupled-device (CCD) detector. The studied crystals were mounted in a continuous-flow temperature-regulated liquid nitrogen cryostat and a polarized 632.8 nm He–Ne laser line, focused to a few micron spot diameter, was used for excitation. In addition to the doped samples, Raman active phonons of oriented Y_2SiO_5 have been studied and used as a template.

For the infrared measurements, the samples were mounted on a closed cycle cryostat cold finger and 0.25 cm^{-1} resolution transmission spectra at $T = 8.5$ up to 150 K were obtained

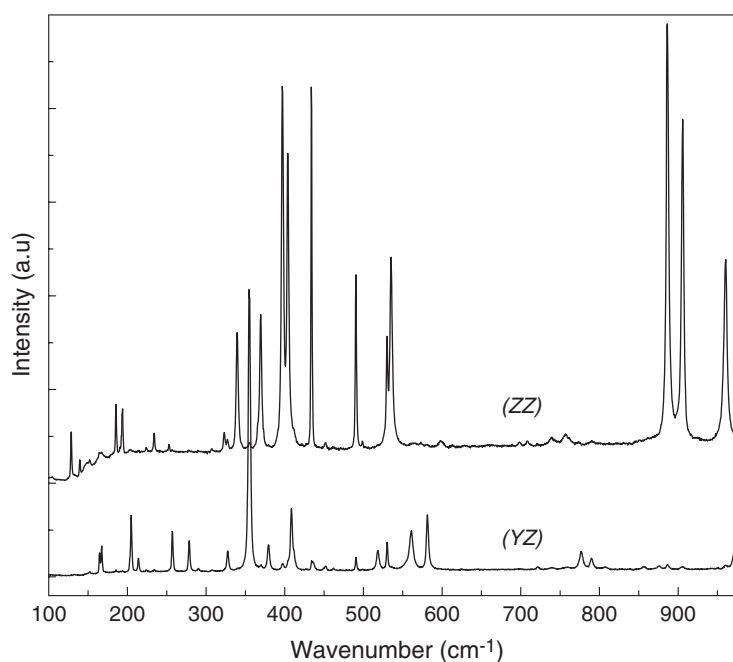


Figure 1. YSO Raman spectra at 77 K for two different polarization configurations: $X(ZZ)X(A_g)$ and $X(YZ)X(B_g)$.

Table 1. Main bands observed in the Raman spectra of undoped YSO compound.

Symmetry	Wavenumbers (cm ⁻¹)
A _g	129, 140, 185, 191, 194, 225, 234, 253, 290, 323, 340, 370, 397, 404, 427, 535, 564, 599, 887, 906, 943, 960
B _g	153, 164, 167, 203, 204, 214, 257, 279, 307, 327, 355, 380, 409, 518, 554, 560, 581, 971

in the 9000–15000 cm⁻¹ energy range using a Fourier transform interferometer (BOMEM DA3.002) equipped with a quartz–halogen source, a quartz beamsplitter and a Si detector.

3. Raman spectroscopy

Figure 1 presents the Raman spectra at liquid nitrogen temperature of the YSO crystal for two different polarization configurations: $X(ZZ)X$ and $X(YZ)X$, which select the A_g and B_g modes respectively. In the unit cell with C_{2h}⁶ space group, the low point group symmetry leads to the following Γ point irreducible representations [10–12]: $\Gamma = 48A_g + 48B_g + 48A_u + 48B_u$. Hence, a very large number of bands are expected in the Raman spectra for the two configurations. In table 1 we report the A_g and B_g phonon frequencies of figure 1. As shown in figure 2, for the 5% and 15% Yb-doped YSO, low frequency phonons are redshifted as expected from the Y³⁺ and Yb³⁺ mass differences. In addition to the frequency redshift, the substitution of Y³⁺ by Yb³⁺ introduces additional broadening (for example, at 4.2 K the 92 cm⁻¹ (FWHM \sim 4.5 cm⁻¹) phonon in 15% Yb:YSO as compared to the 94 cm⁻¹ (FWHM \sim 1.8 cm⁻¹) phonon in undoped YSO).

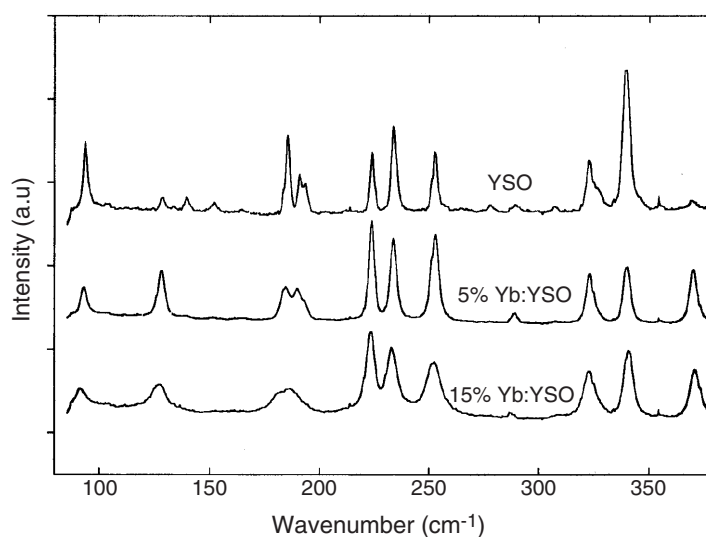


Figure 2. YSO and Yb:YSO low frequency Raman spectra at $T = 4.2$ K.

Raman spectra of 6% Yb:LSO and 1% Yb:SSO were recorded at 78 K in order to study the phonon evolution in the three hosts. The small size of the 1% Yb:SSO sample obtained by the melting zone elaboration process prevents the recording of Raman spectra in distinct polarization configurations and renders the overall comparison mainly qualitative. In figure 3, no analyser was used so that A_g and B_g modes could be detected. Three main phonon groups labelled A, B and C are dominated by Y (Sc, Lu); Y (Sc, Lu)–O, Si–O; and Si–O vibrations respectively. The vibration bands in the 500–700 cm^{-1} range are characteristic of the Y–O vibrations (Y–O₆ octahedra) and their frequencies in the three hosts are related to the reduced mass and the strength of the chemical bonding. The mean cation–oxygen distances (table 2) vary as $d(\text{Y–O}) > d(\text{Lu–O}) > d(\text{Sc–O})$. In a rough estimate, one could predict the phonon frequency of a vibration band to be proportional to the square root of the ratio of the strength of the chemical bonding (proportional to the inverse cation–oxygen distance) over the reduced cation mass. Also, the ionic radii for the rare earth cations vary similarly to the cation–oxygen distances ($r(\text{Y}) = 1.04 \text{ \AA} > r(\text{Lu}) = 1.00 \text{ \AA} > r(\text{Sc}) = 0.89 \text{ \AA}$) and the masses as $M(\text{Lu}) > M(\text{Y}) > M(\text{Sc})$. Hence, for the yttrium and lutetium ions, the mass variation is partly compensated by the changes of the chemical bonding. In contrast, for the scandium compound, the mass and $d(\text{Sc–O})$ distances combine to blueshift the $\nu(\text{Sc–O})$ frequency vibrations. This is observed in figure 3, where the M–O vibrations shift, for instance, from 599 and 625 cm^{-1} in YSO and LSO respectively to 644 cm^{-1} in SSO.

4. Infrared transmission

A sketch of the Yb^{3+} energy levels in a lower than cubic symmetry is given in figure 4. At very low temperature, the lowest crystal field component of the $^2F_{7/2}$ ground state (labelled 0) is the only populated one. Therefore, one expects three absorption lines (for each Yb site) connecting the 0 sublevel to the 0', 1' and 2' CF levels of the $^2F_{5/2}$ excited state. The 8.8 K experimental transmission spectra of Yb: YSO, LSO and SSO (5, 6 and 1% respectively) are presented in figure 5. For the three compounds, the absorption lines occur in three spectral ranges labelled R_1 , R_2 and R_3 that correspond to the $0 \rightarrow 0'$, $1'$ and $2'$ transitions respectively.

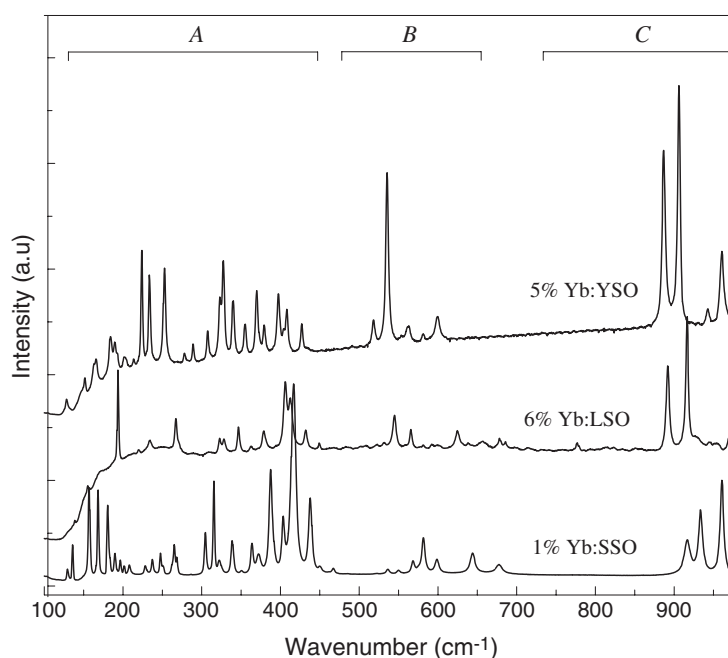


Figure 3. 5% Yb:YSO, 6% Yb:LSO, 1% Yb:SSO, A_g and B_g Raman active phonons at 77 K.

Table 2. Mean cation–oxygen distances and standard deviation (in brackets) for the two rare earth sites in the orthosilicates, and rare earth ionic radii (coordination number 6); $r(\text{Yb}^{3+}) = 1.01 \text{ \AA}$. For site I, with a coordination number 6 + 1, the most remote oxygen has not been included in the mean distance calculation. See the text for the SSO distance calculation.

Compounds	Mean rare earth–oxygen distance and (standard deviation) (\AA)		Rare earth radius (\AA)	Reference
	Site I	Site II		
YSO	2.309 (0.084)	2.269 (0.029)	1.04	[11]
LSO	2.277 (0.060)	2.229 (0.030)	1.00	[12]
SSO	2.204 (0.059)	2.159 (0.039)	0.89	

There are two main lines in the R_1 range, indicating that Yb³⁺ ions enter the two non-equivalent RE sites (I and II) in each lattice. Several weaker satellites of the main bands can be seen in the three spectra (figure 5). They will be discussed in the next section of the paper. Intensities of the two main lines in R_1 , R_2 and R_3 spectral ranges are similar for Yb:YSO and Yb:LSO. However, in Yb:SSO, spectrum lines labelled II are significantly weaker than lines I. This indicates that the relative population of site II is smaller in this compound. Table 2 gives the mean RE–oxygen distances and ionic radii in the three lattices. Using the LSO structure [13] and the unit cell parameters of SSO [14], we have calculated the Sc–O distances that would occur if the real SSO structure were simply homothetic of LSO. Since the Yb³⁺ ionic radius ($\sim 1.01 \text{ \AA}$), is very similar to those of Y³⁺ and Lu³⁺, it is likely that the Yb³⁺ substitute statistically these two cations with equal distributions over the two sites. In contrast, Sc³⁺ is significantly smaller and one can imagine that Yb³⁺ preferentially enters the Sc³⁺ site I which is larger and more distorted than site II [14]. Actually, in the investigation of Er³⁺:SSO [14],

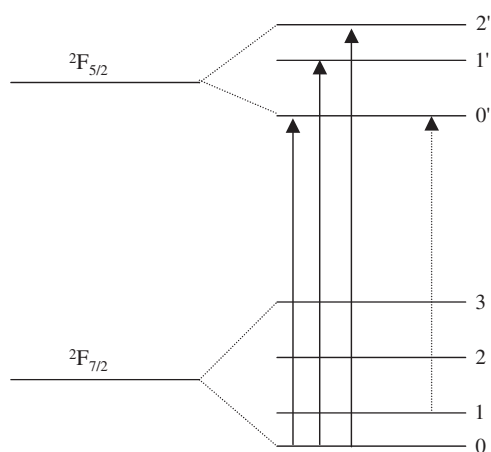


Figure 4. Energy level diagram for the Yb^{3+} ion in a lower than cubic symmetry site.

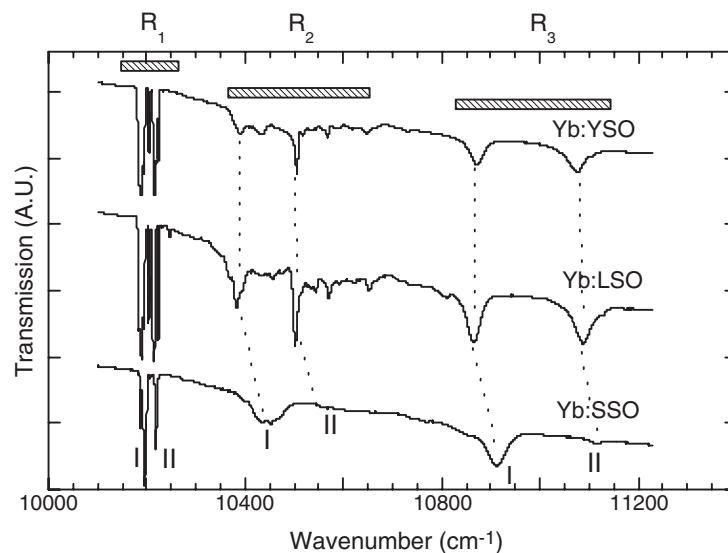


Figure 5. Infrared transmission spectra of $\text{Yb:M}_2\text{SiO}_5$, $M = \text{Y, Lu and Sc}$ recorded at 8.8 K. I and II correspond to the Yb^{3+} ions' two non-equivalent sites. R_1 , R_2 and R_3 label the three spectral ranges associated with the $0 \rightarrow 0'$, $0 \rightarrow 1'$ and $0 \rightarrow 2'$ transitions respectively.

it was noticed that Er^{3+} , whose ionic radius ($\sim 1.03 \text{ \AA}$) is very similar to the Yb^{3+} ionic radius, preferentially substitutes one of the two Sc^{3+} sites of the SSO lattice. It is straightforward, from this preferential site occupation, to assign the two sites' $0 \rightarrow 2'$ transitions (R_3 spectral range) in the three compounds, as indicated in figure 4. The case of the $0 \rightarrow 1'$ lines in the R_2 spectral range is more complicated, since they are superimposed on the phonon replica of the $0 \rightarrow 0'$ lines.

An enlarged R_2 zone transmission spectrum of $\text{Yb}^{3+}:\text{YSO}$ is given in figure 6, together with the YSO ($A_g + B_g$) Raman spectrum. The observed infrared active vibronic sidebands result from the coupling between the odd parity infrared active CF excitations and the even parity Raman active phonons. For the sake of comparison, the origin of the absorption spectrum

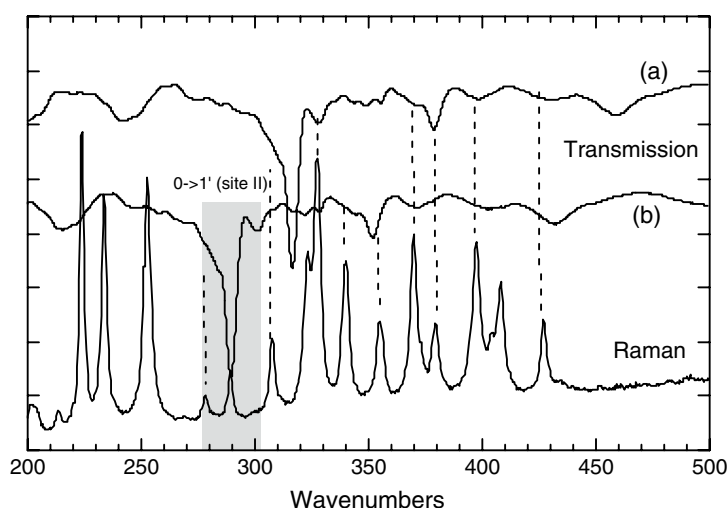


Figure 6. 5% Yb:YSO electronic transmission spectra at 8.8 K with the origin at the $0 \rightarrow 0'$ line for site I (a) and II (b) as compared to the Raman active phonon spectrum at 77 K. Dashed curves indicate the $0 \rightarrow 0'$ transition phonon side-bands. The grey area shows a resonance between the site II $0 \rightarrow 1'$ transition and a YSO phonon.

has been taken at the $0 \rightarrow 0'$ lines of sites I and II respectively. The lines that coincide in energy in the absorption and Raman spectra are assigned to phonon satellites. We are left with the pure electronic $0 \rightarrow 1'$ line, which does not correspond to the Raman spectrum (case of site I) or which is particularly intense because of a resonance with a phonon excitation (case of site II in figure 6). Weak oscillations around $11\,150\text{ cm}^{-1}$, in the tail of the $0 \rightarrow 2'$ site II absorption line (figure 5), are also probably vibronic sidebands of the $0 \rightarrow 0'$ line coupled to the strong A_g Raman modes at 887 and 906 cm^{-1} .

The absorption spectra were also recorded upon warming the samples from 8.8 up to 150 K . The lines remain sufficiently narrow in this temperature range to allow the observation of new lines originating from the ${}^2F_{7/2}$ Yb³⁺ ground-state sublevel 1 (figure 4). For instance site I, $1 \rightarrow 0'$ and $1 \rightarrow 2'$, and site II, $1 \rightarrow 0'$, transitions are clearly identified in the 5% Yb:YSO (figure 7) spectra, allowing the positioning of the two site levels 1.

Similar procedures have been applied to the Yb:LSO and Yb:SSO absorption spectra with the levels given in table 3. These results are compared with published data when available, since the Yb:LSO absorption spectra are, to our knowledge, reported here for the first time. The Yb:YSO energy level diagram at 15 K has been reported by Haumesser *et al* [7]; while the ${}^2F_{5/2}$ total splittings are identical, the absolute values of the $0'$ and $2'$ level energies differ by $5\text{--}8\text{ cm}^{-1}$. However, the discrepancy is larger for levels $1'$, which are identified in [7] at additional $+30$ and $+12\text{ cm}^{-1}$ for sites I and II respectively. The difference between the two studies may be due in part to spectrometer calibration problems and also to a difference in the sample temperatures. For levels $1'$, it may also have been difficult to recognize the pure electronic transitions from the phonon replica.

The Yb:SSO diagram at 27 K has also been reported very recently [8]. The agreement with our data is fair, with some differences in the sublevel positions ($\sim 2\text{--}20\text{ cm}^{-1}$) except for the site I $2'$ level which is reported at $10\,862\text{ cm}^{-1}$ in [8] while observed at $10\,912\text{ cm}^{-1}$ in the present study. One may suspect an error in [8], since their standard deviation of the theoretical calculations for the site I energy levels is 17.7% , in contrast to only $1\text{--}6\%$ for the other seven reported compounds.

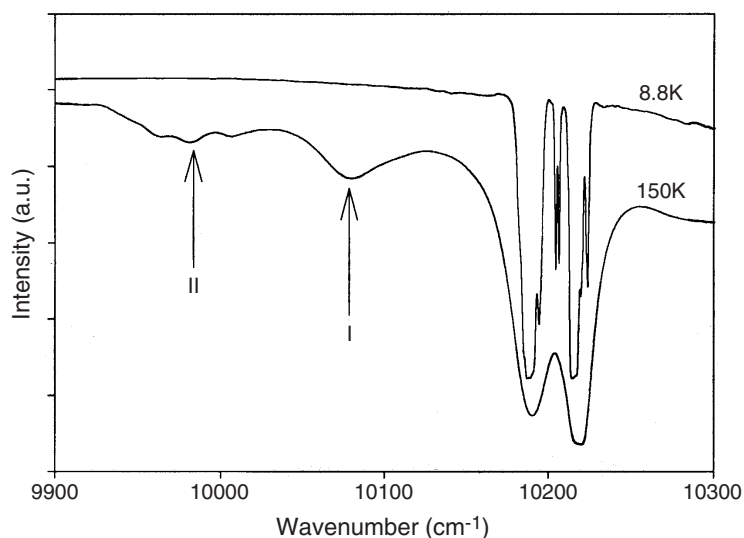


Figure 7. 5% Yb:YSO electronic transmission spectra at 8.8 and 150 K. Arrows indicate the $1 \rightarrow 0'$ transitions for both sites I and II.

Table 3. Energy of the Yb^{3+} CF sublevels deduced from the absorption spectra for the three rare earth orthosilicate hosts. $\Delta(^2F_{5/2})$ designates the total splitting of the $^2F_{5/2}$ state.

Compound	RE site	$^2F_{5/2}$ sublevels (cm^{-1})			$\Delta(^2F_{5/2})$ (cm^{-1})	$^2F_{7/2}$ sublevel 1 (cm^{-1})
		$0'$	$1'$	$2'$		
Yb:YSO	I	10 189	10 390	10 872	683	110
	II	10 216	10 505	11 077	861	237
Yb:LSO	I	10 189	10 383	10 864	675	92
	II	10 214	10 502	11 088	874	—
Yb:SSO	I	10 196	10 454	10 912	716	131
	II	10 219	10 739	11 115	896	—

In the three studied compounds, the total splitting of the $^2F_{5/2}$ state, which reflects the crystal-field strength experienced by the Yb^{3+} ions, is larger for site II as compared to site I (table 3). This can be related to the fact that the rare earth–oxygen distances in the coordination polyhedra (table 2) are smaller in site II as compared to site I, leading to a stronger crystal field. In a similar way, the $\text{Yb}^{3+} ^2F_{5/2}$ overall splittings for sites I and II in Yb:SSO are significantly larger than for Yb:YSO and Yb:LSO, reflecting the strain that the SSO lattice exerts on the Yb^{3+} ions due to the large difference between the Sc^{3+} and Yb^{3+} ionic radii (table 2). In contrast, the modification of the RE ionic radii and the corresponding bond lengths in Yb:YSO and Yb:LSO are not sufficient to induce an important modification of the crystal field strength and its associated splitting (see table 3).

Table 4 summarizes the $^2F_{5/2}$ splittings for Yb^{3+} ions substituted for the rare earth or alkaline earth cations in several materials for which laser emission has been demonstrated [9]. It can be seen that the splittings observed here in the RE orthosilicates fall within the largest ones, especially for Yb:SSO. This indicates that these high crystal field strength materials would also exhibit large overall splittings of the ground state and low or negligible thermal population

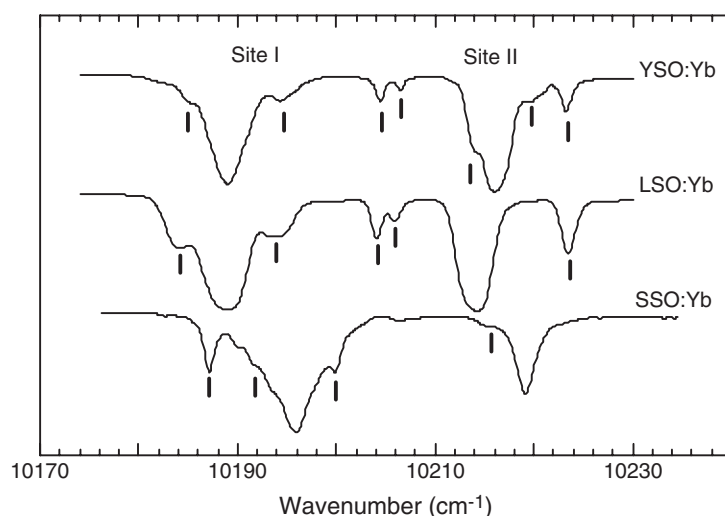


Figure 8. Expanded view of the infrared transmission spectrum R_1 range for both Yb³⁺ sites in Yb:YSO, Yb:LSO and Yb:SSO. The vertical lines designate some of the satellites of the main $0 \rightarrow 0'$ lines.

Table 4. Total splitting of the Yb³⁺ $^2F_{5/2}$ state $\Delta(^2F_{5/2})$ [9] when inserted in various oxide lattices of interest for laser applications.

Compound	KGd(WO ₄) ₂	Y ₃ Al ₅ O ₁₂	Y ₂ O ₃	Sr ₃ Y(BO ₃) ₃	Ca ₄ Gd(BO ₃) ₃ O	Sr ₅ (VO ₄) ₃ F
$\Delta(^2F_{5/2})$ (cm ⁻¹)	494	575	433 and 784	679 and 764	843	909

of the terminal level in quasi-three-level laser operation. This explains why Yb:YSO has already shown interesting laser properties described in the introduction, and also why Yb:LSO and Yb:SSO, which furthermore present quite large thermal conductivity [8], are promising materials for high power laser operation.

5. Satellites of the main absorption lines

In addition to the main absorption lines corresponding to the $0 \rightarrow 0'$ transitions of Yb(I) and Yb(II), several weaker lines are observed, in the same spectral range, for the three studied compounds. This is shown in figure 8 which presents the 8.5 K transmission spectra of YSO:5% Yb, LSO:6% Yb and SSO:1% Yb. The first two spectra are very similar but the third one is markedly different. As pointed out before, in Yb:SSO the Sc³⁺ site (II) is less substituted by Yb³⁺ as compared to the Sc³⁺ site (I) and the satellites around the $0 \rightarrow 0'$ site (I) main line are more numerous than in the other two compounds.

The satellite lines may be due to the presence of impurities (other rare earth) in the compounds, but this is unlikely because large amount of impurities would be required, since several satellites have areas of the order of 5–8% of the main lines.

The observation of satellites in the absorption spectra of lanthanide-doped compounds is a fairly common phenomenon which has been extensively studied in materials such as garnets or rare earth sesquioxides [15], in Nd³⁺ activated YVO₄ and YLiF₄ [16] and in Nd:Ca₄M(BO₃)₃O, M = Gd, Y [17]. They have been interpreted in terms of (i) perturbed

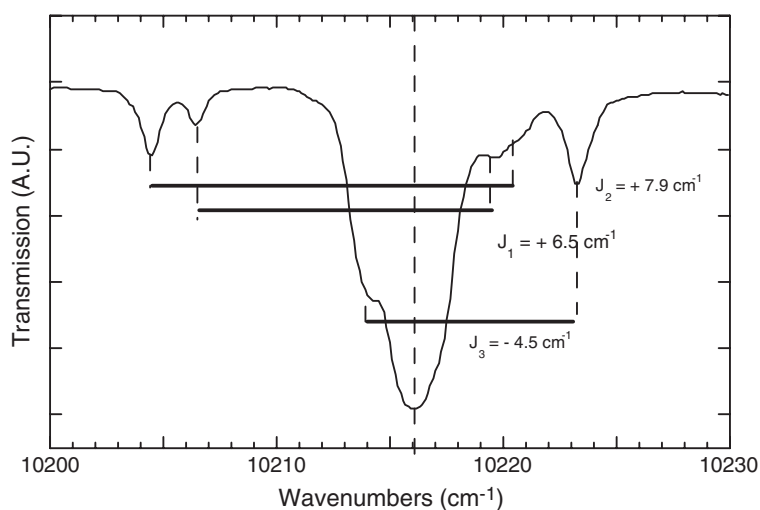


Figure 9. Expanded Yb:YSO absorption spectrum showing the $0 \rightarrow 0'$ site II transition and a tentative interpretation of the satellites on the basis of $\text{Yb}^{3+}\text{--Yb}^{3+}$ magnetic interactions.

sites associated with lattice defects [17], (ii) modification of the crystal field at the lanthanide site due to the formation of ion pairs [15] and (iii) occurrence of magnetic exchange coupling between lanthanide ions in pairs [16]. In Yb^{3+} -doped compounds, ion pairing was also observed and evidenced mainly through cooperative absorption or luminescence effects [18–20]. Interestingly, Yb^{3+} dimers were also shown to be involved in optical bistability phenomena [21].

In the present case, two interpretations may be considered: a crystal field perturbation at the main sites due to the presence of Yb^{3+} ions at neighbouring sites or a magnetic coupling between $\text{Yb}^{3+}\text{--Yb}^{3+}$ pair ions. Y(I) and Y(II) ions have respectively seven and six yttrium neighbours at distances shorter than 4.15 \AA with which they share one or two oxygens (see table 5). It follows that the influence of such an Yb^{3+} ion in the first cationic coordination sphere of another yttrium ion is likely to be important.

Since the perturbing ions would be located at several sites close to a given Yb^{3+} , several satellites for each site main line should result, depending on the pair distances and bondings. *Ab initio* crystal field calculations based on electrostatic interaction may eventually allow a further description of their origin.

Concerning the second possibility dealing with magnetic interactions between neighbouring Yb^{3+} ions, Guillot-Noël *et al* [16] have shown that two satellites must be observed at $\Delta + J/2$ and $\Delta - 3J/2$ where Δ corresponds to the isolated ion CF transition energy and J corresponds to the pair exchange coupling constant ($J > 0$ for ferromagnetic interactions). On this basis, a tentative assignment of the main satellites for Yb:YSO site II is proposed as an example in figure 9. Three different ytterbium pairs with $J_1 = 6.5$, $J_2 = 7.9$ and $J_3 = -4.5 \text{ cm}^{-1}$ could be identified, indicating that $\text{Yb}^{3+}\text{--Yb}^{3+}$ pairs would possibly undergo ferromagnetic and antiferromagnetic interactions. These pairs may correspond to three of the five possible edge-sharing polyhedra given in table 5 around site II. In favour of this interpretation is the assignment of all the observed satellites. Furthermore, the J values are comparable with those reported for neodymium pairs in YVO_4 and YLiF_4 [16] and for Yb–Yb pairs in SrF_2 [22]. Zeeman effect and EPR measurements [16, 23, 24] would be particularly helpful to validate the $\text{Yb}^{3+}\text{--Yb}^{3+}$ pair magnetic interactions.

Table 5. Yttrium–yttrium distances in YSO according to the structural data given in [11]. The table is limited to the eighth neighbour and the connection between the Y coordination polyhedra (edge or corner, or no common oxygen) is indicated in each case.

		Neighbour number							
		1	2	3	4	5	6	7	8
Y(I)	Type of neighbour	Y(II)	Y(II)	Y(I)	Y(II)	Y(I)	Y(I)	Y(II)	Y(II)
	Distance (Å)	3.395	3.507	3.621	3.721	3.791	4.031	4.145	4.695
	Link to Y(I)	Edge	Edge	Edge	Edge	Edge	Edge	Corner	None
Y(II)	Type of neighbour	Y(I)	Y(II)	Y(I)	Y(II)	Y(I)	Y(I)	Y(I)	Y(I)
	Distance (Å)	3.395	3.459	3.507	3.623	3.721	4.145	4.695	4.949
	Link to Y(II)	Edge	Edge	Edge	Edge	Edge	Corner	None	None

6. Conclusion

A detailed investigation of the low temperature infrared absorption spectra of Yb:YSO, Yb:LSO and Yb:SSO has led to a precise identification of the crystal field excitation of Yb³⁺ ions in the two sites of the three crystalline hosts. Following the detection of the Raman active phonons of the hosts, these excitations have been clearly distinguished from the phonon replica observed in the same spectral range. It turns out that the Yb³⁺ ions experience high crystal field strength, especially in the case of Yb:SSO. This may be important for the applications of these quasi-three-level laser systems.

Also, weak satellites appearing in the absorption spectra have been detected for the first time in the rare earth orthosilicates. They may be attributed to perturbed Yb³⁺ sites or to magnetically coupled Yb³⁺–Yb³⁺ pairs.

Acknowledgments

We thank J Rousseau and M Castonguay for technical assistance, Olivier Guillot-Noël, Marina Popova and Andrée Kahn-Harari for fruitful discussion regarding the pair spectra and the crystal structures of the rare earth orthosilicates. S Campos, A Denoyer and S Jandl acknowledge support from the National Science and Engineering Research Council of Canada and the Fonds Québécois de la Recherche sur la Nature et les Technologies.

References

- [1] De Loach L D, Payne S A, Chase L L, Smith L K and Kway W L 1993 *IEEE J. Quantum Electron.* **29** 1179
- [2] Gaumé R, Haumesser P-H, Viana B, Vivien D, Ferrand B and Aka G 2002 *Opt. Mater.* **19** 81
Mougel F, Dardenne K, Aka G, Kahn-Harari A and Vivien D 1999 *J. Opt. Soc. Am. B* **16** 164
- [3] Gapontsev V and Krupke W 2002 *Laser Focus World* (August) 83
Krupke W F 2000 *IEEE* **6** 1287
- [4] Gaumé R, Haumesser P-H, Aka G, Viana B, Vivien D, Scheer E, Bourdon P, Ferrand B, Jacquet M and Lenain N 2000 *Trends Opt. Photon.* **34** 469
- [5] Haumesser P-H, Gaumé R, Viana B and Vivien D 2002 *J. Opt. Soc. Am. B* **19** 2365

- [6] Chénais S, Druon F, Balembois F, Lucas-Leclin G, Fichot Y, Georges P, Gaumé R, Viana B, Aka G and Vivien D 2003 *Opt. Mater.* **22** 129
- [7] Haumesser P-H, Gaumé R, Viana B, Antic-Fidancev E and Vivien D 2001 *J. Phys.: Condens. Matter* **13** 5427
- [8] Gaumé R, Viana B, Derouet J and Vivien D 2003 *Opt. Mater.* **22** 107
- [9] Gaumé R 2002 *PhD Thesis* Paris VI University
- [10] Jacquemet M, Balembois F, Chénais S, Druon F, Georges P, Gaumé R, Viana B, Vivien D and Ferrand B 2003 *Trends Opt. Photon.* **83** 184
- [11] Ellens A, Andres H, Meijerink A and Blasse G 1997 *Phys. Rev. B* **55** 173
- [12] Maksimov B A, Ilyukhin V V, Kharitonov U A and Belov N V 1970 *Kristallografiya* **15** 926
- [13] Gustafsson T, Klintonberg M, Derenzo S E, Weber M J and Thomas J O 2001 *Acta Crystallogr. C* **57** 668
- [14] Liddell K and Thompson D 1986 *Trans. J. Br. Ceram. Soc.* **85** 17
- [15] Lupei A and Lupei V 2003 *Opt. Mater.* **24** 181
- [16] Guillot-Noël O, Metha V, Viana B, Gourier D, Boukhris M and Jandl S 2000 *Phys. Rev. B* **61** 15338
- [17] Lupei A, Antic-Fidancev E, Aka G, Vivien D, Aschehoug P, Goldner P, Pellé F and Gheorghe L 2002 *Phys. Rev. B* **65** 224518
- [18] Noginov M A, Loutts G B, Steward C S, Lucas B D, Fider D, Peters V, Mix E and Huber G 2002 *J. Lumin.* **96** 129
- [19] Goldner P, Schaudel B and Prassas M 2002 *Phys. Rev. B* **65** 054103
- [20] Montoya E, Espeso O and Bausá L E 2000 *J. Lumin.* **87–89** 1036
- [21] Hehlen M P, Gudel H U, Shu Q and Rand S C 1996 *J. Chem. Phys.* **10** 1232
- [22] Velter-Stefanescu M, Nistor S V and Grecu V V 1986 *Phys. Rev. B* **34** 1459
- [23] Metha V, Guillot-Noël O, Gourier D, Ichalalène Z, Castonguay M and Jandl S 2000 *J. Phys.: Condens. Matter* **12** 7149
- [24] Guillot-Noël O, Goldner P, Higel P and Gourier D 2003 *Chem. Phys. Lett.* **380** 563